Beeson, H.W., and McCoy, S.W., 2021, Disequilibrium river networks dissecting the western slope of the Sierra Nevada, California, USA, record significant late Cenozoic tilting and associated surface uplift: GSA Bulletin, https://doi.org/10.1130/B35463.1.

Supplemental Material

Figure S1. Analytical solution for knickpoint elevation (Equation 11 in main document) for a range of *K* values showing that when uplift is nonuniform, knickpoint elevation depends on *K* as well as the new uplift rate.

Figure S2. χ plots for stable upland basins underlain by the Sierra batholith that were used to back-calculate *K* from *k*sn (the slope of the regression line) using published catchment-average erosion rates.

Figure S3. Slope-area plots of lower sections of major river basins that are characteristic of equilibrated reaches proximal to the mountain front along the Sierra Nevada, ordered from north to south.

Figure S4. χ plots for the American River in the northern Sierra (A) and the Kings River in the southern Sierra (B) for multiple values of Θ.

Figure S5. Proposed stream capture of previously closed basins in the upper Feather River basin.

Figure S6. Mainstem tectonic knickpoint locations relative to mean channel steepness.

Figure S7. Field photos of the lower Kaweah River showing exposed bedrock downstream of the 'mainstem tectonic knickpoint'.

Figure S8. Conceptual schematic showing how variability in measurements of incision into basement rock below Mio-Pliocene volcanic deposits arise owing to location of modern rivers relative to paleorivers.

Figure S9. Spatial gradient in incision in to basement rock below ridges downstream of mainstem knickpoints projected to the crest.

Figure S10. Mainstem knickpoint elevations and uplift rates from linked 1-D simulations of an equilibrated river network subject to rigid-block forward tilting with a linear background uplift rate and vertical beds of varying width and erodibility.

Figure S11. Transient river incision rates in the Sierra and the influence of soft bands of rock on river profiles.

Figure S12. Results from 1-D river simulations of multiple tilting events adapted from Beeson and McCoy (2020).

Text. Derivations of equations for knickpoint locations.

kmz files.

Supplemental Material for *Disequilibrium river networks dissecting the western slope of the Sierra Nevada, California record significant late Cenozoic tilting and associated surface uplift*

Helen W. Beeson and Scott W. McCoy

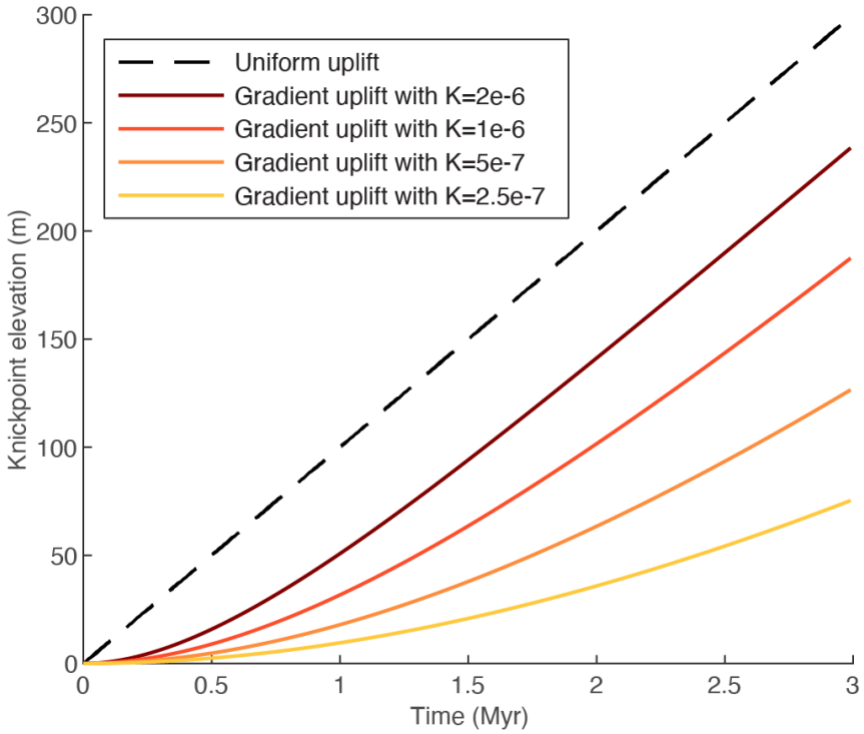

Figure 1. Analytical solution for knickpoint elevation (Equation 11 in main document) for a range of K values showing that when uplift is nonuniform, knickpoint elevation depends on K as well as the new uplift rate. Note that this analytical solution required parameter values (specifically m, h, and k_a) that are different than those used in our numerical simulations.

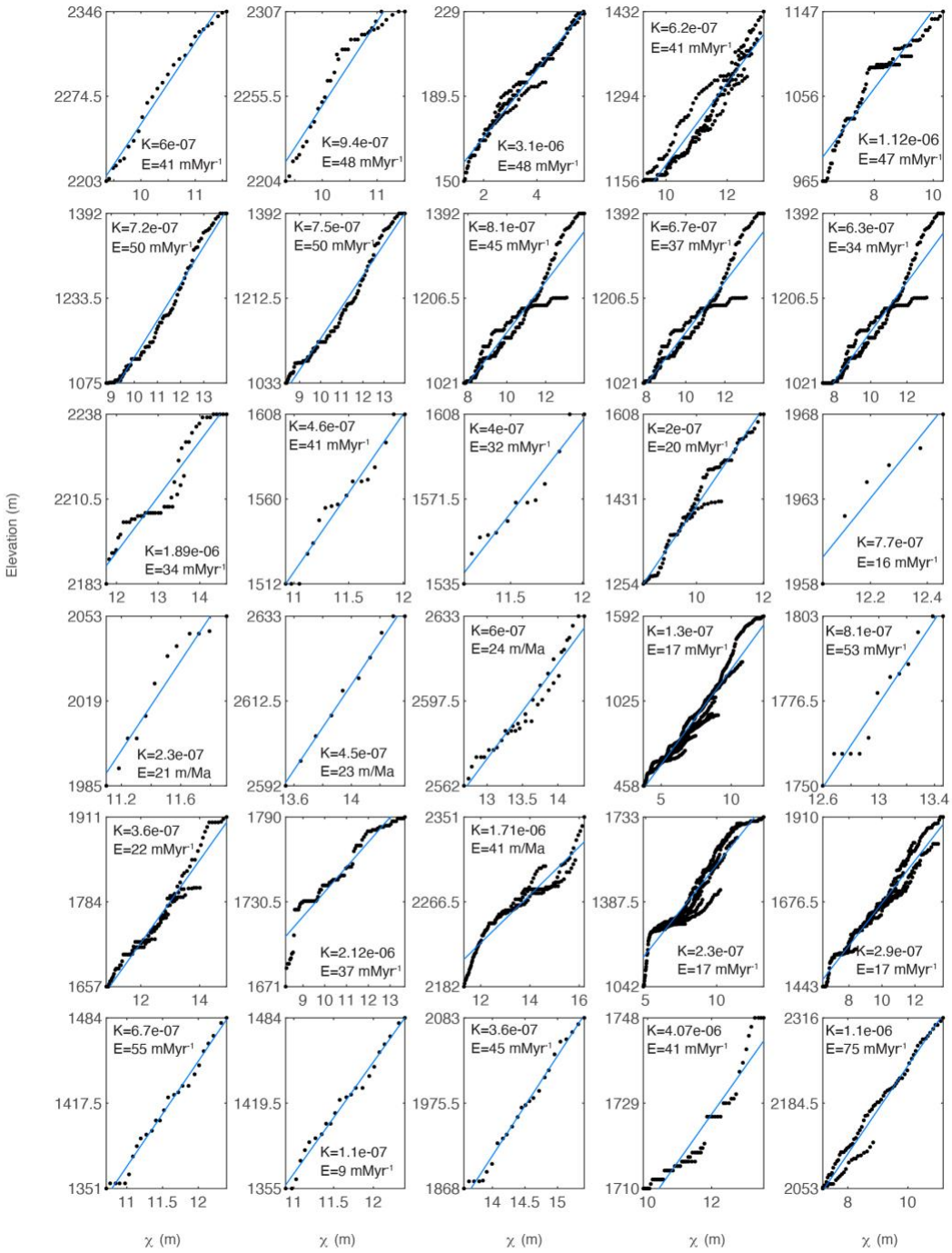

Figure 2. χ plots for stable upland basins underlain by the Sierra batholith that were used to back-calculate K from k_{sn} (the slope of the regression line) using published catchment-average erosion rates. Erosion rates were measured from upland granitic soil-mantled basins and rates were adjusted for chemical erosion (Callahan et al., 2019).

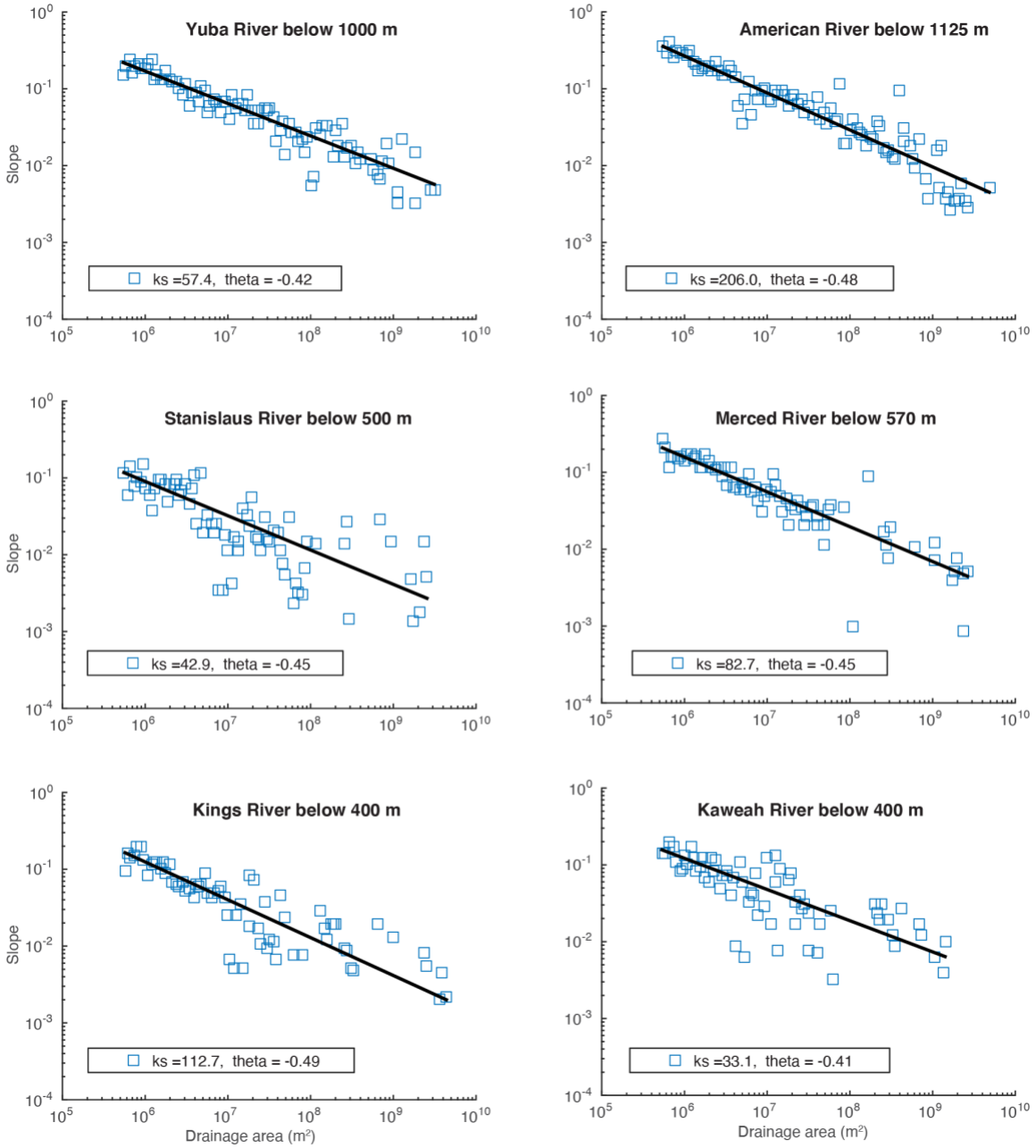

Figure 3. Slope-area plots of lower sections of major river basins that are characteristic of equilibrated reaches proximal to the mountain front along the Sierra Nevada, ordered from north to south. These plots demonstrate consistent slope-area scaling and a narrow range of concavity, θ, on which we based our choice of θ=0.45 for all further analysis, models, and χ maps.

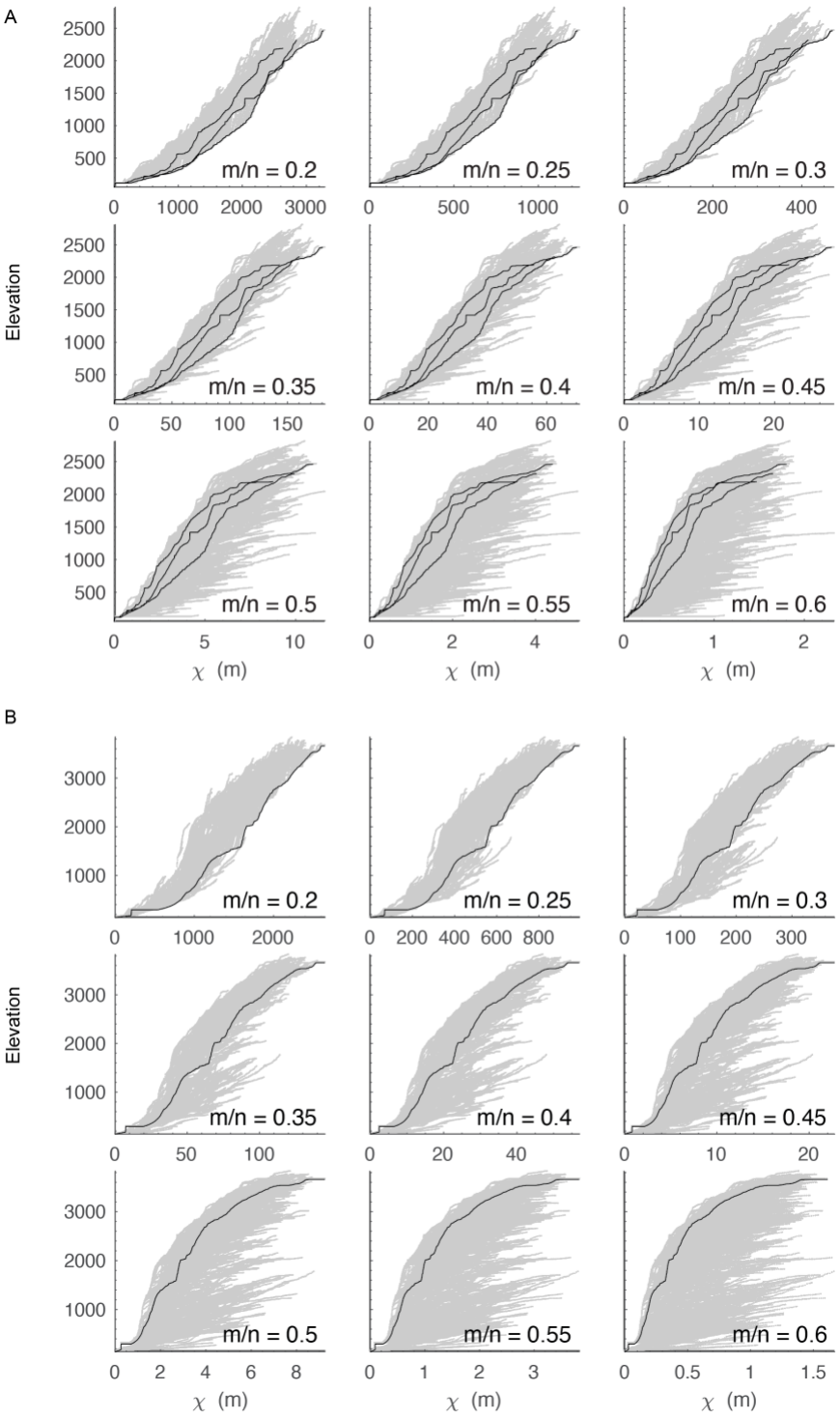

Figure 4. χ plots for the American River in the northern Sierra (A) and the Kings River in the southern Sierra (B) for multiple values of θ.

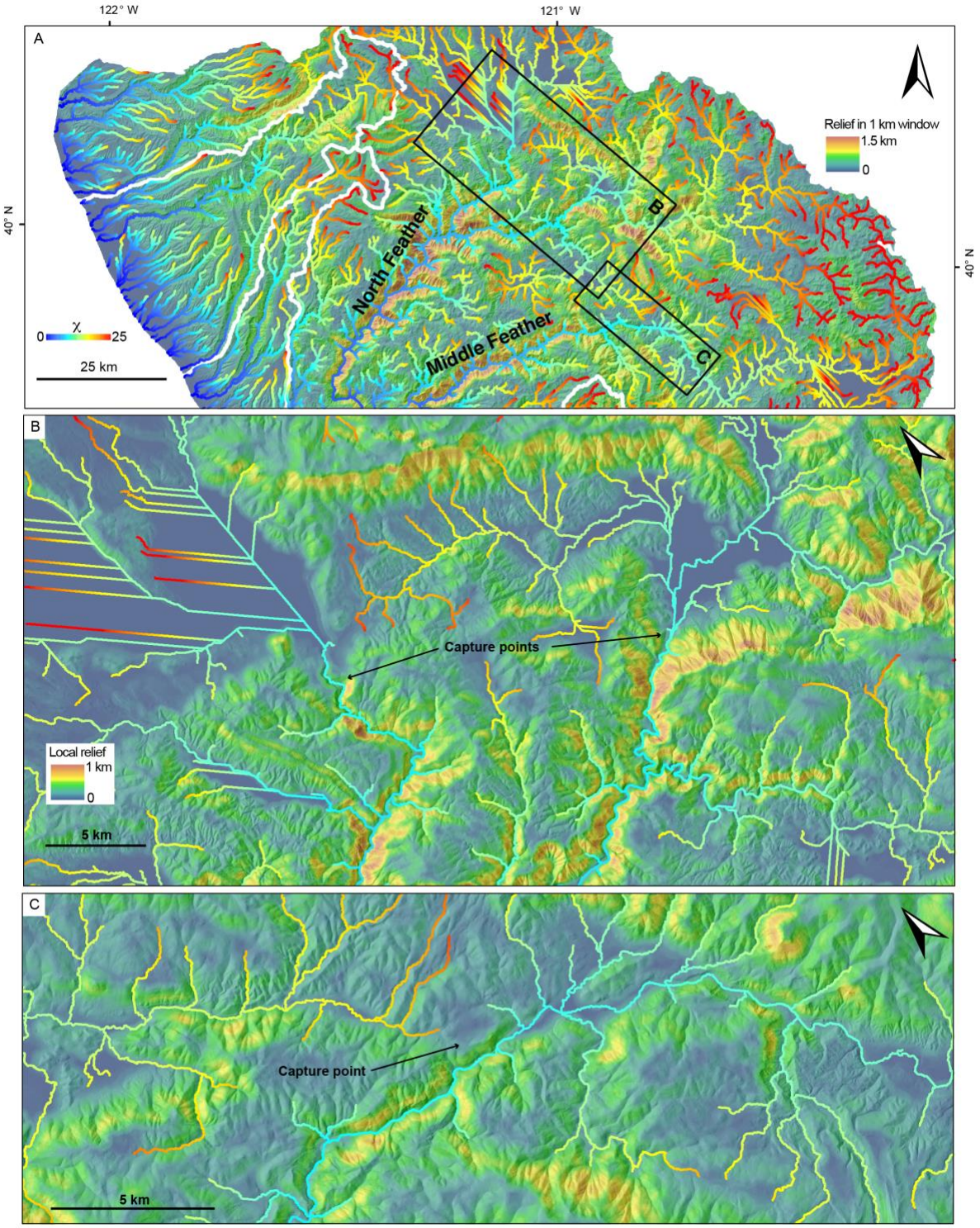

Figure 5. Proposed stream capture of previously closed basins in the upper Feather River basin. A. χ map of Feather River basin and capture points (in pink) in the North and Middle Feather Rivers. B. Shaded-relief image showing detail around capture points in the upper North Fork Feather. Low-relief areas above pink markers are the closed basins proposed to be captured. C. Shaded-relief image with capture point (in pink) in the upper Middle Fork Feather overlaying χ map. Dashed arrow shows proposed paleoriver flow path of a tributary of the Middle Fork Feather that used to drain to the North Fork Feather.

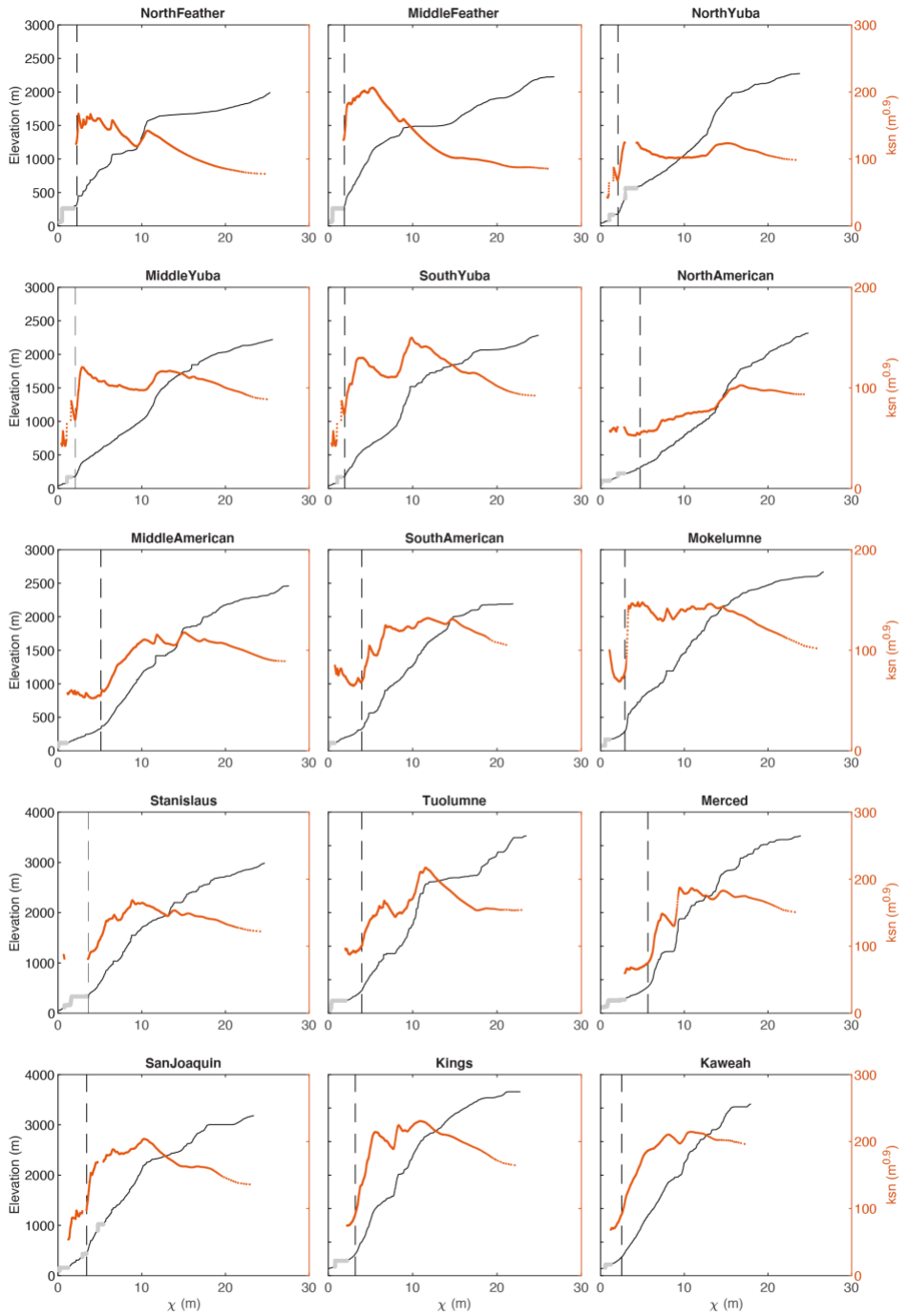

Figure 6. Mainstem tectonic knickpoint locations relative to mean channel steepness. χ-elevation plot is shown in black. The orange line shows mean k_{sn} that is calculated by progressively adding more points moving away from the mountain front, excluding points that fall within reservoirs. The locations of the mainstem tectonic knickpoints in each river, shown with dashed black vertical lines, generally falls at a minimum of mean k_{sn} just downstream of a rapid increase.

A

B

Figure 7. Field photos of the lower Kaweah River showing exposed bedrock downstream of the ‘mainstem tectonic knickpoint’. A. Photo taken looking upstream at 36° 26' 17.742" N, 118° 54' 22.62" W. B. Photo taken looking upstream at 36° 24' 40.932" N, 118° 56' 22.2" W.

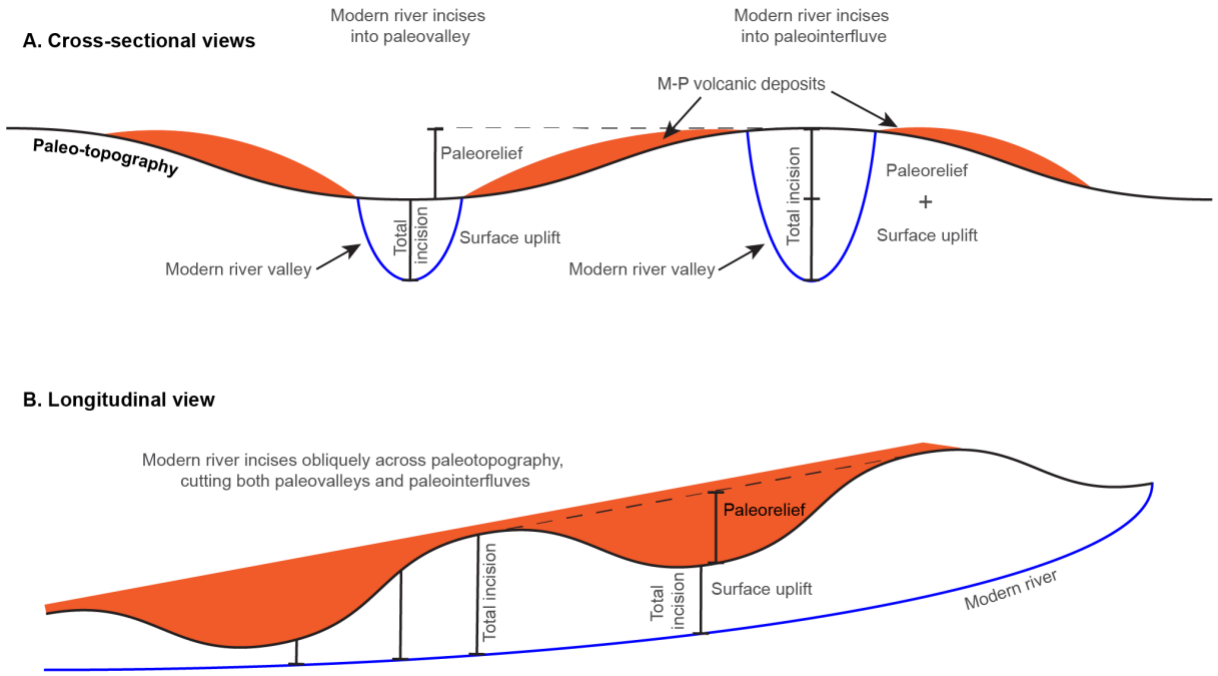

Figure 8. Conceptual schematic showing how variability in measurements of incision into basement rock below Mio-Pliocene volcanic deposits arise owing to location of modern rivers relative to paleorivers. A. Cross-sectional views of a modern river incising into a paleo-valley, creating relatively low values of incision as measurements do not incorporate any paleorelief (left) and a modern river incising into a paleointerfluve, creating relatively high values of incision as measurements incorporate paleorelief (right). B. Longitudinal view of a modern river cutting obliquely across paleotopography and incising both paleovalleys and paleointerfluves, creating longitudinal variability in measured incision values.

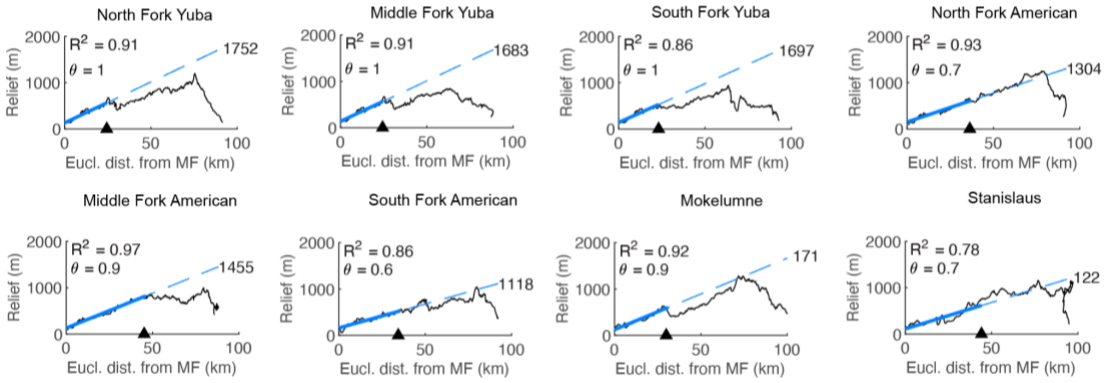

Figure 9. Spatial gradient in incision into basement rock below ridges downstream of mainstem knickpoints projected to the crest (supplemental insets for Fig. 11).

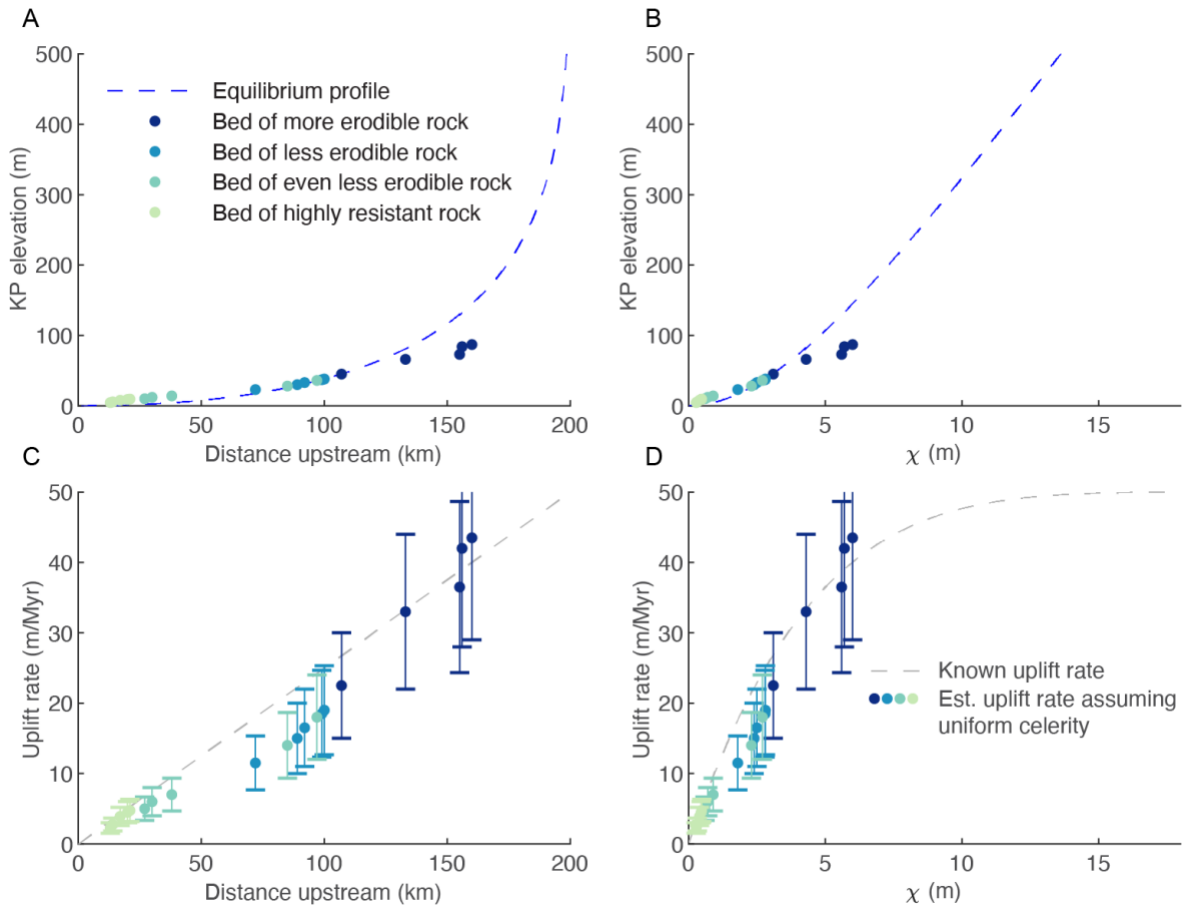

Figure 10. Mainstem knickpoint elevations and uplift rates from linked 1-D simulations of an equilibrated river network subject to rigid-block forward tilting with a linear background uplift rate and vertical beds of varying width and erodibility. Simulations were stopped and knickpoint elevations were recorded at t = 3 Myr following tilting. Uplift rate is estimated by dividing knickpoint elevation by 3 Myr (time since cessation of tilting) and multiplying by a factor of 1.5. Error bars represent the uncertainty in the value of this conversion factor, which ranges from 1 to 2, depending on how the knickpoint traverses the uplift field. Knickpoint elevations and associated uplift rate estimates are plotted against distance upstream (A, C) and χ (B, D).

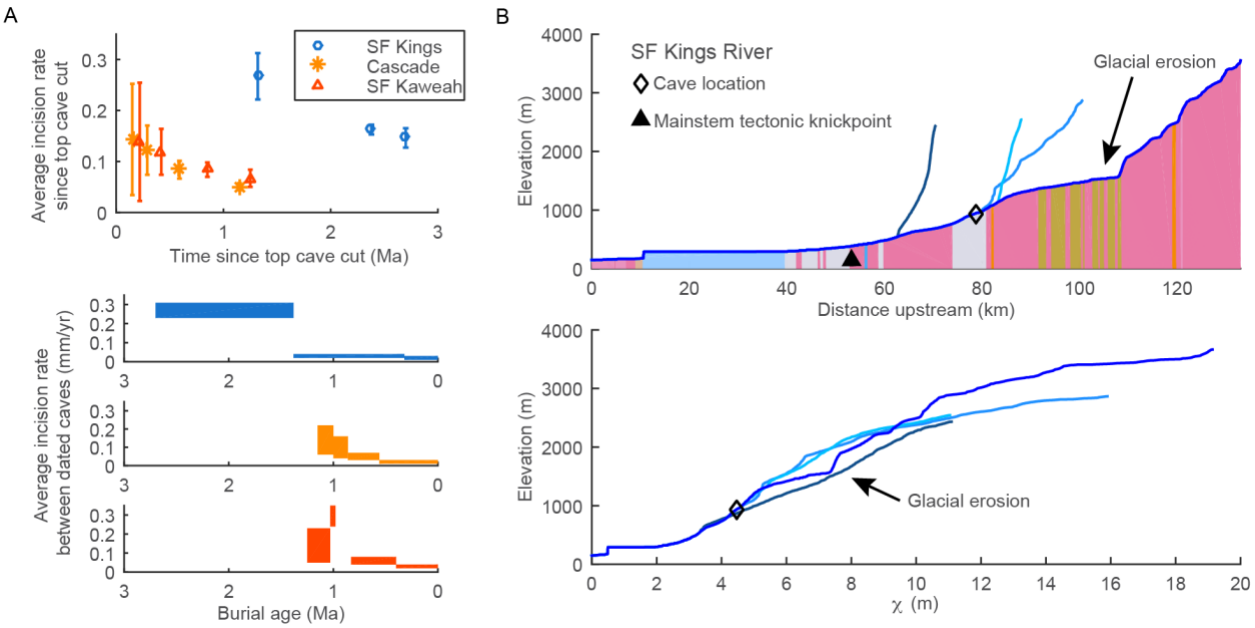

Figure 11. Transient river incision rates in the Sierra and the influence of soft bands of rock on river profiles. A. River incision rates for the South Fork Kings River, Cascade Creek, and South Fork Kaweah River adapted from Stock et al. (2004, 2005). B. Longitudinal profiles (upper) and χ plots (lower) of mainstem South Fork Kings and three tributaries with surface geology (Ludington et al., 2005) of mainstem under longitudinal profile (see Fig. 2 for rock type legend). Approximate cave system location projected to longitudinal profile from Stock et al. (2004, 2005) shown with a black diamond.

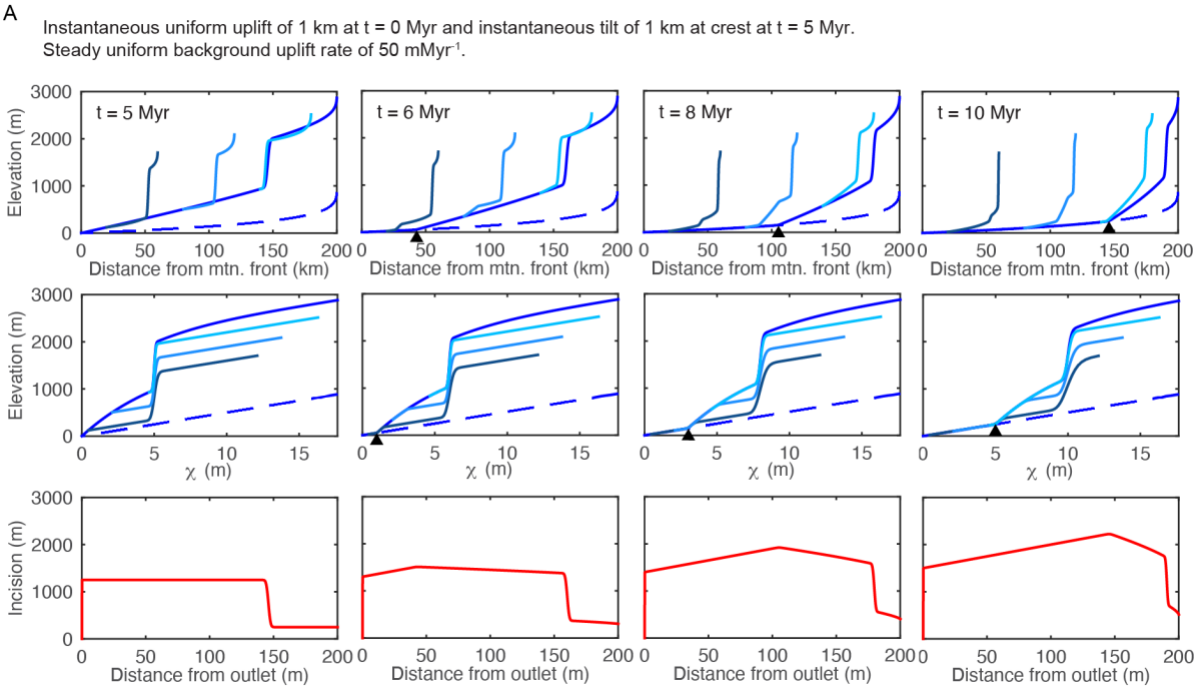

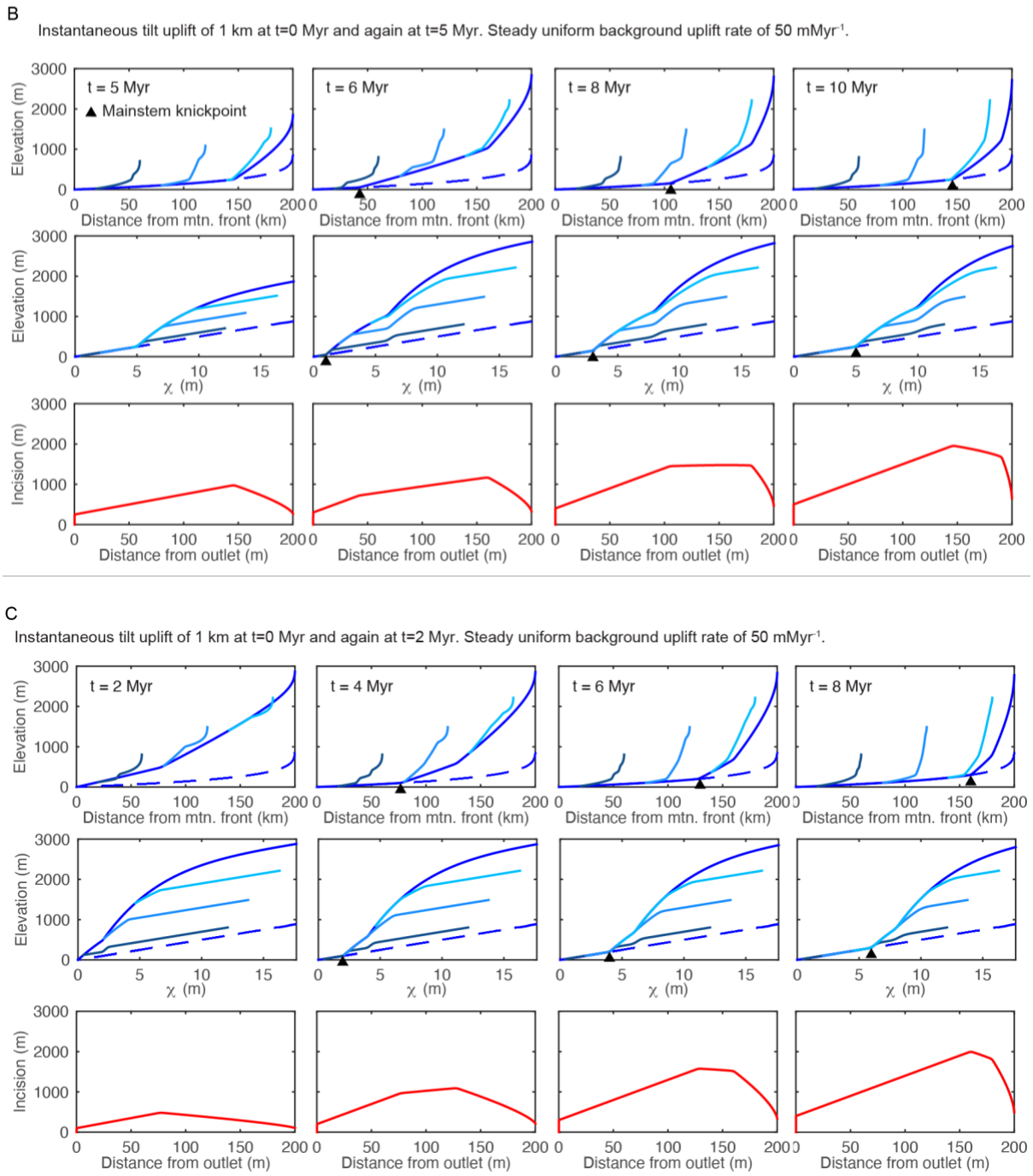

Figure 12. Results from 1-D river simulations of multiple tilting events adapted from Beeson and McCoy (2020). A. Uniform pulse of uplift of 1 km at *t*=0 Myr and instantaneous tilt of 1 km at the crest at *t*=5 Myr. B. Instantaneous tilt of 1 km at *t*=0 Myr and an instantaneous tilt of 1 km at *t*=5 Myr. C. Instantaneous tilt of 1 km at *t*=0 Myr and an instantaneous tilt of 1 km at *t*=2 Myr. Upper rows of plots show longitudinal profiles, the middle rows show χ plots, and the lower rows show incision below the elevation of the mainstem longitudinal profile, "paleo-topography", since *t*=0 Myr. See Fig. 3A for schematic of 1-D model setup.

Derivations of equations for knickpoint locations

Beeson, H.W. and McCoy, S.W.

1 Horizontal knickpoint location

We begin with the equation for channel response time (Main document Equation 6) rewritten for knickpoint location upstream of a base level at $x = 0$:

$$\tau(x_{kp}) = \int_0^{x_{kp}} \frac{1}{KA^m S^{n-1}} dx \tag{1}$$

We make the following assumptions:
1) Drainage area can be described by Hack's Law: $A = k_a(L - x)^h$
2) K is spatially uniform
3) $n = 1$
4) $m = 0.5$
5) $h = 2$

These allow us to simplify the integral to

$$\tau_{kp} = \frac{1}{{k_a}^m K} \int_0^{x_{kp}} \frac{1}{L - x} dx \tag{2}$$

Solving the definite integral and replacing τ with t gives us an equation for knickpoint location in terms of distance upstream as a function of time, t:

$$x_{kp}(t) = L(1 - e^{-{k_a}^m Kt}) \tag{3}$$

We now take the equation for χ

$$\chi_{kp} = \int_0^{x_{kp}} \frac{1}{A(x)^m} dx \tag{4}$$

which simplifies to

$$\chi_{kp} = \frac{1}{{k_a}^m} \ln\left(\frac{L}{L - x_{kp}}\right) \tag{5}$$

substituting Equation 3 for x_{kp} and simplifying yields

$$\chi_{kp} = Kt \tag{6}$$

2 Vertical knickpoint location

When $n = 1$, only the new uplift rate matters as wave speed (and therefore the position of the knickpoint on the new equilibrium profie) is not dependent on channel slope. We therefore only consider the new uplift field here.

2.1 The new uplift field, U_2, is spatially uniform

Knickpoints mark the most upstream end of a new equilibrium river profile, so we can use the equation for steady-state river elevation (Equation 4 from the main document) to write an equation for knickpoint elevation:

$$z_{kp} = \left(\frac{U_2}{K}\right) \int_0^{x_{kp}} \frac{1}{A(x)^m} dx \tag{7}$$

The integral portion is the same as that in Equation 4, thus we can substitute in its solution (Equation 6) and we get the expected result that knickpoint elevation depends only on the new uplift rate (e.g., Mitchell and Yanites, 2019):

$$z_{kp} = U_2 t \tag{8}$$

2.2 The new uplift field, U_2, is an uplift gradient

Here we assume that the new uplift field, U_2 can be described as:

$$U_2(x) = \alpha x + U_0 \tag{9}$$

Rewriting Equation 7 for this case yields

$$z_{kp} = \frac{1}{K} \int_0^{x_{kp}} \frac{U_2(x)}{A(x)^m} dx \tag{10}$$

Substituting in Equation 9 and Hack's Law yields

$$z_{kp} = \frac{1}{{k_a}^m K} \int_0^{x_{kp}} \frac{\alpha x + U_0}{L - x} dx \tag{11}$$

Solving the definite integral and simplifying, we get

$$z_{kp} = \frac{U_0}{{k_a}^m K} \ln\left(\frac{L}{L - x_{kp}}\right) + \frac{\alpha}{{k_a}^m K} \left(L \ln\left(\frac{L}{L - x_{kp}}\right) - x_{kp}\right) \tag{12}$$

Substituting χ_{kp} in where the right side of Equation 5 appears:

$$z_{kp} = \frac{U_0}{K} \chi_{kp} + \frac{\alpha}{K} \left(L\chi_{kp} - \frac{x_{kp}}{{k_a}^m}\right) \tag{13}$$

Simplifying, and substituting Kt for χ_{kp}

$$z_{kp}(t) = t(U_0 + \alpha L) - \frac{\alpha x_{kp}}{k_a K} \tag{14}$$

Identifying U_L as the uplift rate at the channel head:

$$U_L = U_0 + \alpha L \tag{15}$$

Substituting this in as well as Equation 3 for x_{kp} and simplifying yields

$$z_{kp}(t) = U_L t - \frac{U_L - U_0}{{k_a}^m K} \left(1 - e^{-{k_a}^m K t}\right) \tag{16}$$